Mid-Infrared Intersubband Cavity Polaritons in Flexible Single Quantum Well

*Puspita Paul[1], Sadhvikas J. Addamane[2], Peter Qiang Liu [1,]**

[1]Department of Electrical Engineering, University at Buffalo, The State University of New York, Buffalo, NY 14260, USA

[2]Center for Integrated Nanotechnologies, Sandia National Laboratories, Albuquerque, NM 87123, USA

KEYWORDS: light-matter interaction, ultrastrong coupling, semiconductor quantum well, intersubband transition, polariton, mid-infrared, flexible substrate

ABSTRACT

Strong and ultrastrong coupling between intersubband transitions in quantum wells and cavity photons have been realized in mid-infrared and terahertz spectral regions. However, most previous works employed a large number of quantum wells on rigid substrates to achieve coupling strengths reaching the strong or ultrastrong coupling regime. In this work, we experimentally demonstrate ultrastrong coupling between the intersubband transition in a single quantum well and the resonant mode of photonic nanocavity at room temperature. We also observe strong coupling between the nanocavity resonance and the second-order intersubband transition in a single quantum well. Furthermore, we implement for the first time such intersubband cavity polariton systems on soft and flexible substrates, and demonstrate that bending of the single quantum well does not significantly affect the characteristics of the cavity polaritons. This work paves the way to broaden the range of potential applications of intersubband cavity polaritons, including soft and wearable photonics.

TEXT

Strong light-matter interactions underlie the operations of various photonic and optoelectronic devices. Resonant photonic cavities with small volume and/or high quality factor can significantly enhance intrinsically weak light-matter interactions via the Purcell effect.[1,2] When the coupling between a matter excitation and a resonant photonic cavity mode becomes sufficiently strong, the rate of energy exchange between the matter excitation and the cavity mode can exceed the damping rate of either, leading to the formation of two hybrid excitations composed of partial light and partial excited matter.[3-12] In such a scenario, the system is in the strong coupling regime and the hybrid light-matter excitations are often referred to as cavity polaritons. The frequency difference between the two polariton modes is referred to as the Rabi splitting, which is twice the Rabi frequency Ω_{Rabi} and represents the coupling strength of the light-matter interaction. When the light-matter interaction is so strong that the Rabi splitting becomes a significant fraction of the original matter excitation frequency, the system enters the so-called ultrastrong coupling regime.[13-18] Strong coupling and ultrastrong coupling regimes have been realized for a variety of material platforms and matter excitations, such as electronic transitions in atoms,[4] excitons in semiconductors,[5-7,18] phonons in solids[8,9] and vibrational modes in molecules,[10,11] cyclotrons in two-dimensional electron gas,[17] as well as qubits based on Josephson junctions.[12,16]

Another technologically important system of material and matter excitation for studying and utilizing such cavity quantum electrodynamics is the intersubband transitions (ISTs) in semiconductor quantum wells (QWs).[19] Thanks to the highly flexible band structure engineering for QW structures, ISTs can cover the majority of the terahertz (THz) to mid-infrared (MIR) spectral region and are the foundation of two crucial device technologies: quantum cascade laser (QCL) [20,21] and quantum well infrared photodetector (QWIP).[22,23] Furthermore, IST cavity polaritons can be exploited for a variety of MIR and THz device applications, such as realizing unconventional light sources,[24,25] photodetectors,[26] and optical switches/modulators.[27,28] In recent years, strong coupling and ultrastrong coupling between cavity photons and individual ISTs have been demonstrated using different photonic cavity structures containing multiple QWs (MQWs) with high doping concentrations.[15,24-33] Although MQWs facilitate the realization of strong

coupling as the coupling strength is proportional to $\sqrt{N}$ (N is the number of repeated QWs),[30] the growth of MQWs can be more complex and challenging than growing a single QW (SQW). In addition, the operation principles of some IST-based devices favor fewer number of QWs. For instance, the key performance metrics of QWIP are largely inverse proportional to the number of QWs.[23,34] Furthermore, thinner semiconductor heterostructures such as a SQW are more suitable for realizing soft and flexible devices, as they generally can withstand more strain than MQWs. Furthermore, SQW-based structures allow for effective field effect tuning of the carrier density which can lead to electrically reconfigurable devices, whereas field effect tuning of the carrier densities in MQWs is difficult or infeasible due to the interlayer screening of the electric field. However, it is significantly more challenging to reach the same coupling strength in an SQW-based system than in an MQW-based system. Previous studies have also shown that when a QW is relatively wide and/or heavily doped to have carriers occupying multiple subbands, the Coulomb dipole-dipole interaction induces coherence between different individual ISTs and cause them to merge into a single high-energy multisubband plasmon (MSP),[35,36] which eventually transitions into a Berreman mode as the QW becomes much wider.[37,38] Exceedingly strong interactions between cavity photons and the MSP or Berreman mode have been demonstrated. For example, strong coupling with 13% normalized Rabi splitting was achieved for the MSP excitation in an SQW[35] and ultrastrong coupling with 33% normalized Rabi splitting was achieved for the MSP excitation in an MQWs structure (5 QWs),[36] whereas the normalized Rabi splitting was further increased to 73% for the Berreman mode in a 148 nm wide SQW[37] and to 91% for the Berreman mode in a structure consisting of 5 QWs of 148 nm wide.[38] Nevertheless, strong and ultrastrong coupling between cavity photons and an individual IST in an SQW has not yet been demonstrated. On the other hand, all previous demonstrations of IST cavity polaritons were realized using semiconductor QW structures on rigid substrates, whereas it is not clear whether such delicate physical systems (with nanometric semiconductor layers) can be implemented on soft and flexible substrates and withstand significant deformations which would be required for soft and wearable photonics applications.

In this work, we experimentally demonstrate ultrastrong coupling between an individual MIR IST in a GaAs SQW and the resonant mode of photonic nanocavity at room temperature. The largest ratio between the Rabi splitting $2\Omega_{\mathrm{Rabi}}$ and the measured IST frequency (i.e., the normalized Rabi splitting) reaches 24%, which to the best of our knowledge is the first demonstration of ultrastrong coupling for an individual IST in an SQW. Note that an individual IST still involves the collective oscillation of all the electrons in the subbands. In addition, strong coupling between the nanocavity mode tuned to higher frequencies and the second-order IST (i.e., the IST between the second and third subbands) in an InGaAs SQW is also observed, despite the significantly lower carrier density associated with the second-order IST. Furthermore, in sharp contrast to previous works, we implement these SQW IST cavity polariton systems on soft and flexible substrates and show that even large bending of these SQW-based structures does not significantly affect the characteristics of the IST cavity polaritons. This work may pave the way to broaden the range of potential applications of IST cavity polaritons, such as various soft and wearable photonic devices and systems. For example, flexible and electrically tunable MIR filters, reflectors, or thermal emitters can be used for thermal camouflage applications,[39] and flexible QWIP focal plane arrays can be integrated on curved surfaces to realize compound-eye type imaging systems.

We employed two types of III-V semiconductor SQW structures, i.e., GaAs/$Al_{0.3}Ga_{0.7}As$ SQW grown on a GaAs substrate and lattice-matched $In_{0.53}Ga_{0.47}As/In_{0.52}Al_{0.48}As$ SQW grown on an InP substrate (see Supporting Information). Assuming all the free carriers from ionized dopants are in the SQW, the nominal sheet carrier density in the GaAs SQW is $4.4 \times 10^{12}\ \mathrm{cm}^{-2}$, and the nominal sheet carrier density in the InGaAs SQW is $6.9 \times 10^{12}\ \mathrm{cm}^{-2}$. However, as these SQWs are located relatively close to the semiconductor surface (see Supporting Information) which has high-density surface states that can trap a significant amount of free carriers, the actual sheet carrier density in the SQWs should be a fraction of the above nominal values. The band structures and envelope wave functions of the subbands in these two SQWs are shown in Figure 1a and Figure 1b, respectively. A key difference between these two SQWs is that the GaAs SQW has two quantum confined subbands, whereas the InGaAs SQW has three quantum confined subbands. Therefore, the GaAs SQW can be considered a two-level system which has one IST. On the other

hand, the InGaAs SQW can be considered a three-level system which has two allowed ISTs, i.e., the first-order IST between the first and second subbands, and the second-order IST between the second and third subbands. We characterized the IST absorption spectra of both SQW samples using the conventional multi-pass total internal reflection measurement configuration (see Supporting Information), and the results are plotted in Figure 1c. An absorption peak (at 930 cm^{-1}) associated with the single IST in the GaAs SQW and two absorption peaks (at 1030 cm^{-1} and 1335 cm^{-1}) associated with the two IST transitions in the InGaAs SQW are clearly observed. All the observed IST absorption peaks have a full-width-at-half-maximum (FWHM) of about 100 cm^{-1}. Note that owing to the relatively high carrier density in these SQW structures, the measured IST absorption frequencies are different from (higher than) the corresponding single-particle transition frequencies as a result of the depolarization shift.[23,29,30]

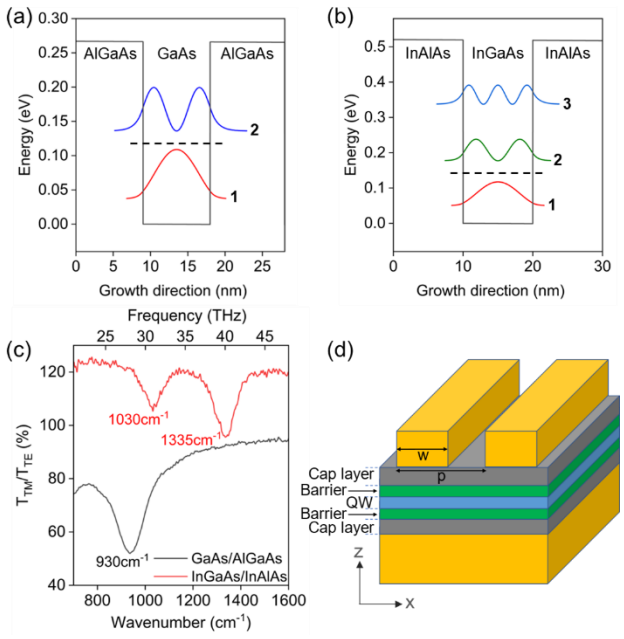

Figure 1 (a) Band structure of the GaAs/AlGaAs SQW with two bound subbands (the square of the envelope wave functions are plotted) leading to a single IST with ~24 THz transition frequency (~100 meV transition energy). (b) Band structure of the InGaAs/InAlAs SQW with three bound subbands (the square of the envelope wave functions are plotted) leading to two ISTs with ~30 THz (~125 meV) and ~39 THz (~163 meV) transition frequencies (transition energies), respectively. The dashed lines in (a) and (b) indicate the approximate Fermi levels calculated based on the

estimated plasma frequency of the 2D electrons in the SQWs. (c) Spectral ratios of the TM-polarization transmission to the TE-polarization transmission for both the GaAs SQW and InGaAs SQW structures. The dips in the spectral ratios represent the IST absorption peaks. The transmission spectra were characterized using the multi-pass total internal reflection sample/measurement configuration. The two spectra are offset by 25% along the y-axis. (d) Schematic of the employed patch antenna nanocavity structures enclosing the SQW heterostructure. In addition to the QW and barrier layers, there are also two thin cap layers in the heterostructure which prevent the oxidation of the barrier layers.

To achieve exceedingly strong light-matter interactions involving the SQW ISTs, we employed resonant nanocavities which are essentially patch antenna structures. Figure 1d illustrates the schematic of the nanocavity structure, which consists of a metal ground plane and a patterned metal strip sandwiching the thin semiconductor layers of the SQW heterostructure. The nanocavity resonance can be excited by an incident light polarized perpendicular to the metal strip. At resonance, the electric field component perpendicular to the semiconductor layers (i.e., E_z) is tightly confined between the metal strip and the ground plane and hence drastically enhanced (see Supporting Information). As E_z is the only field component that can interact with ISTs in QWs, such a patch antenna nanocavity structure is particularly advantageous for achieving strong interactions with ISTs compared to other nanophotonic antenna/resonator designs without a ground plane.

We fabricated two types of samples to demonstrate SQW-based IST cavity polariton systems, i.e., samples based on rigid glass substrates and samples based on soft/flexible polydimethylsiloxane (PDMS) substrates. Figure 2a illustrates the fabrication process for the samples on rigid glass substrates, which is similar to those employed in previous studies.[30,31] The schematics of the step-by-step fabrication process for the samples on flexible PDMS substrates are shown in Figure 2b. The details of the fabrication processes for both types of samples are described in the Supporting Information.

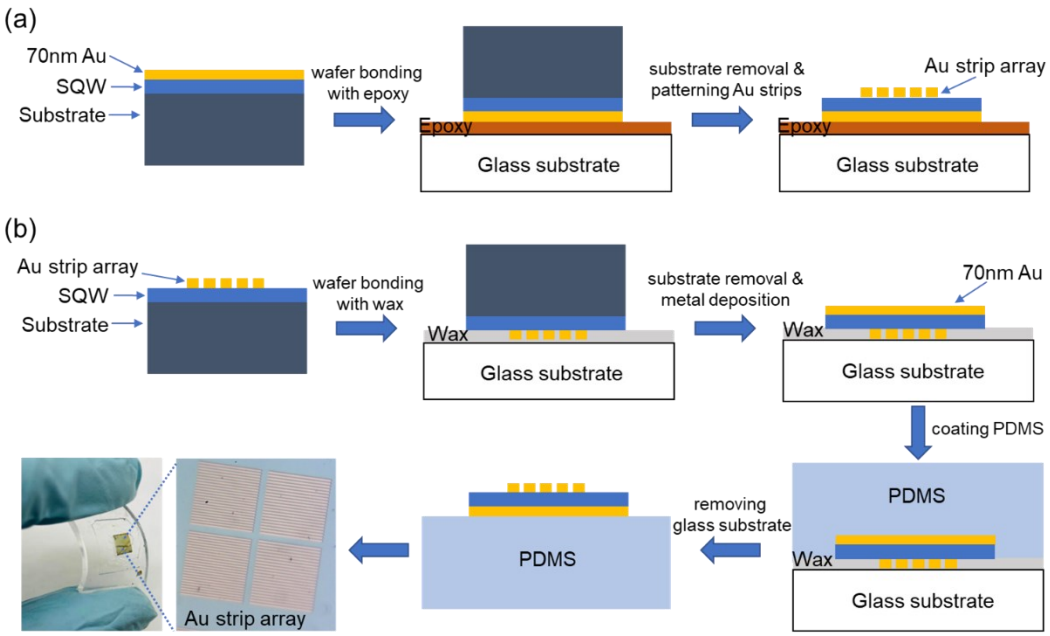

Figure 2 (a) Schematic illustration of the fabrication process for the patch antenna nanocavity structures on rigid glass substrate. (b) Schematic illustration of the fabrication process for the patch antenna nanocavity structures on flexible PDMS substrate. The photo at the end of the chain shows a fabricated sample which was significantly bent.

In general, the strength of light-matter interactions is determined by the local field enhancement experienced by the matter excitation. As the field enhancement inside the patch antenna nanocavity is approximately inverse proportional to the height of the nanocavity, the entire SQW heterostructure should be made as thin as possible to achieve strong or even ultrastrong coupling with the nanocavity resonance mode. Note that the Rabi splitting is proportional to $1/\sqrt{L_{\mathrm{cav}}}$ where L_{cav} is the nanocavity height (see Supporting Information).[30] On the other hand, as III-V semiconductors have relatively high density of surface states that can trap free carriers, the SQW layer should not be too close to the semiconductor surfaces to avoid carrier depletion. Therefore, when it comes to optimizing the total thickness of the SQW heterostructure (i.e., the nanocavity height), the critical trade-off between the nanocavity field enhancement and the free carrier density in the SQW needs to be considered. We investigated the minimum GaAs cap layer thickness that does not cause a significant decrease in the IST absorption signal strength by gradually

reducing the thickness of the upper GaAs cap layer with a digital wet chemical etching process (see Supporting Information). The minimum cap layer thickness was found to be about 10 nm. Reducing the cap layer thickness beyond this limit resulted in a significant decrease of the IST absorption signal strength, likely due to a severe loss of carrier density in the SQW.

To study how the spectral response of the IST-nanocavity system evolves as the nanocavity resonant frequency varies, several arrays of patch antenna nanocavities with different Au strip widths were fabricated on the surface of the SQW heterostructure, and their reflection spectra were characterized using a Fourier transform infrared spectrometer (FTIR, see Supporting Information). The reflection spectra of a set of nanocavity arrays with the specified Au strip widths on a rigid glass substrate are plotted in Figure 3a. The upper and lower GaAs cap layers in these samples were etched down to approximately 14 nm and 10 nm, respectively, making the nanocavity height about 53 nm. It is evident from these reflection spectra that the strong interaction between the IST in the GaAs SQW and the nanocavity resonance leads to the formation of two hybrid modes, i.e., the upper and lower IST polaritons, which manifest themselves as two dips with Lorentzian lineshape in each reflection spectrum. As the nanocavity resonant frequency is varied across the IST frequency, the evolution of the frequencies of the two IST polaritons exhibits typical anti-crossing behavior, which is a signature of the strong and ultrastrong coupling regimes. The minimum frequency difference between the upper and lower polaritons (i.e., the Rabi splitting $2\Omega_{\mathrm{Rabi}}$) is found to be ~220 cm^{-1} (~6.6 THz), which is obtained from the nanocavity array with 1300 nm wide Au strips. This corresponds to a normalized Rabi splitting of 24%, which is in the ultrastrong coupling regime (i.e., normalized Rabi splitting > 20%) according to the conventional definition.[13] A detailed comparison in terms of the normalized Rabi splitting, QW number and doping density between our samples and those reported in numerous representative previous studies are provided in the Supporting Information Table S3. Our result is the first demonstration of the ultrastrong coupling regime for an individual IST (rather than the MSP or Berreman mode excitation) in an SQW.

We further conducted comprehensive simulation of the nanocavity-SQW hybrid system using the finite difference time domain (FDTD) method (see Supporting Information). The simulated reflection spectra of

the experimentally investigated structures are plotted in Figure 3b, which show very good agreement with the corresponding experimental spectra. The near-field profiles of the electric field and electric displacement at the resonance frequencies are included in the Supporting Information. The frequencies of the two IST polaritons as a function of the Au strip width are extracted from Figures 3a-b and plotted in Figure 3c, which again confirm the good agreement between the experiment and simulation. These simulated spectra were obtained by setting a fitting parameter, the plasma frequency ω_p associated with the IST, to 16.8 THz. Based on the measured depolarization-shifted IST absorption frequency ($\widetilde{\omega}_{\mathrm{IST}} \approx$28 THz, see Figure 1c), the corresponding single-particle IST frequency is estimated as $\omega_{\mathrm{IST}} = \sqrt{\widetilde{\omega}_{\mathrm{IST}}^2 - \omega_p^2}$ to be approximately 22.4 THz, which is in good agreement with its design value (24 THz). According to the relationship between the Rabi splitting and the plasma frequency $2\Omega_{\mathrm{Rabi}} = \sqrt{f_{SQW}}\,\omega_p$,[30] the mode overlap factor of the SQW f_{SQW} is estimated to be ~15%, which matches well the ratio between the SQW thickness (9 nm) and the total thickness of the semiconductor heterostructure (53 nm). The small discrepancies between the simulation and experimental results may be due to the inaccuracy of the nanocavity thickness used in the simulation model, which was estimated based on the nominal etching rate of the GaAs cap layers.

The samples on flexible PDMS substrates can be significantly bent without causing any noticeable damage to the SQW and nanocavity structures. Therefore, we characterized the reflection spectra of these samples as they were bent to various extents. Figure 3d shows the reflection spectra of a set of nanocavity arrays with the specified Au strip widths on a PDMS substrate in three different configurations: i.e., flat, bent with 12 mm radius, and bent with 6 mm radius, respectively. The reflection spectra of the sample in all three configurations show clear signatures of IST cavity polaritons in the strong coupling regime, which exhibit the anti-crossing behavior as the nanocavity resonant frequency is varied across the IST frequency. In addition, the frequencies of the IST polaritons (i.e., the positions of the reflection dips) do not show any apparent difference in the different sample configurations, suggesting that the characteristics of these SQW-based IST cavity polaritons are robust to such relatively large bending of the sample. The Rabi splitting

extracted from these sets of spectra is ~146 cm^{-1} (~4.4 THz), which is smaller than that of the sample in Figure 3a. This is mainly because the GaAs spacer layers in this particular sample were thicker (~18 nm), leading to somewhat weaker field enhancement.

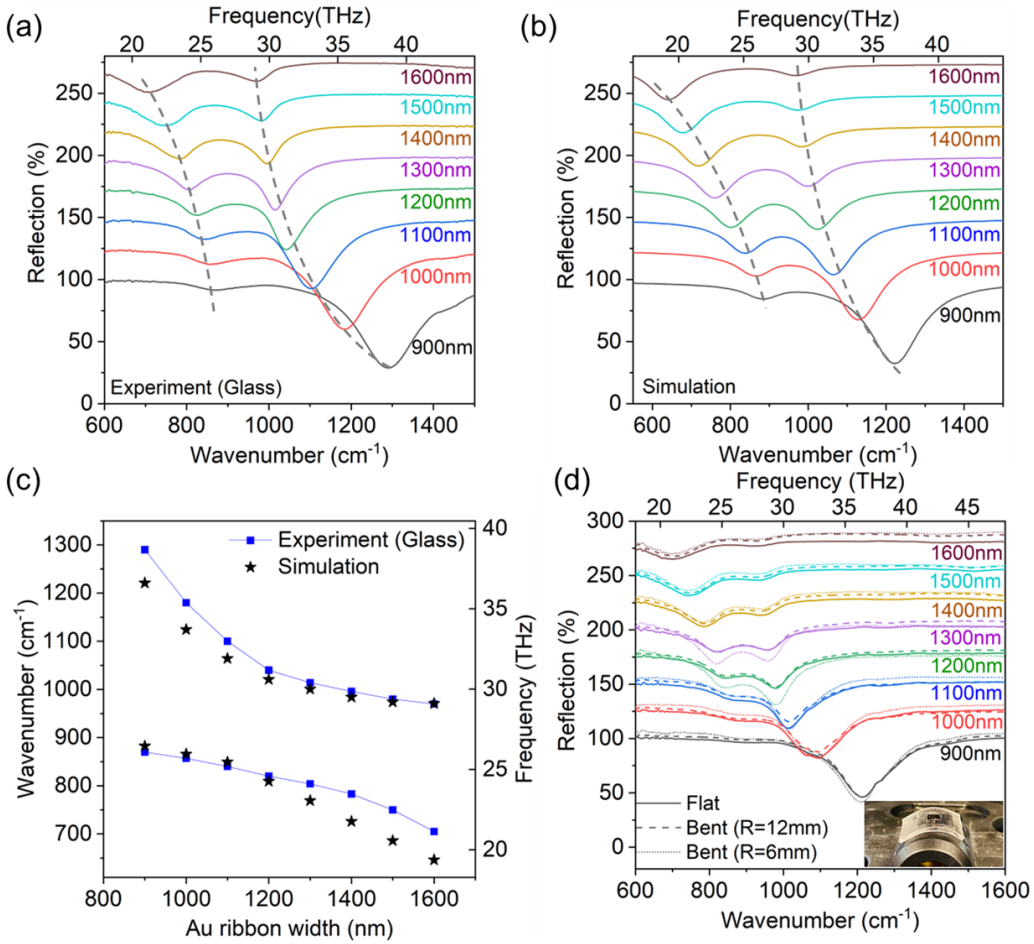

Figure 3 (a) Measured and (b) simulated reflection spectra of different patch antenna nanocavity arrays with various Au strip widths based on the GaAs SQW on glass substrate. The array periodicity is twice the Au strip width. The neighboring spectra are offset by 25% along the y-axis. The dashed lines tracing the polariton peak positions are guides to the eye. (c) Comparison of the experimentally measured IST polariton frequencies (blue squares) extracted from the spectra in (a) with the simulated IST polariton frequencies (black stars) extracted from the spectra in (b). The experimental and simulated results agree well and clearly show the anti-crossing behavior of the two polariton branches. (d) Measured reflection spectra of different patch antenna nanocavity arrays with various Au strip widths based on the GaAs SQW on flexible PDMS substrate in three sample configurations: flat, bent with a 12 mm radius,

and bent with a 6 mm radius. The array periodicity is twice the Au strip width. The neighboring groups of spectra are offset by 25% along the y-axis. Within each group of three spectra (corresponding to the three sample configurations), the spectra are offset by 2% along the y-axis.

We implemented similar patch antenna nanocavity structures for the InGaAs SQW heterostructure on both rigid glass and flexible PDMS substrates, and investigated the strong light-matter interactions between the nanocavity resonance and the two ISTs in the InGaAs SQW. Figure 4a shows the experimental reflection spectra of two different samples each with a set of nanocavity arrays with various Au strip widths. One sample has a rigid glass substrate whereas the other one has a flexible PDMS substrate (in the flat configuration). Both samples show similar reflection spectra as the nanocavity resonant frequency is varied across the two ISTs in the InGaAs SQW. The sample on PDMS substrate exhibits a slightly larger Rabi splitting than the sample on glass substrate, and this small discrepancy might be the result of fabrication variation and/or wafer non-uniformity. In stark contrast to the results obtained from the GaAs SQW-based samples, the reflection spectrum of each InGaAs SQW-based nanocavity array shows three resonances (reflection dips), which is a result of the single nanocavity resonance coupling to two ISTs. When the Au strip width is relatively large (>850 nm), the nanocavity resonance couples strongly to the first-order IST. The corresponding Rabi splitting at the anti-crossing condition (900 nm wide Au strip for the sample on PDMS substrate) is found to be ~5.9 THz (~198 cm^{-1}), which is approximately 19% of the first-order IST frequency and hence entering the ultrastrong coupling regime. When the Au strip width becomes smaller than 850 nm, the nanocavity resonance predominantly couples to the second-order IST, which also leads to two distinctive dips in the reflection spectrum. Therefore, strong coupling is also achieved between the nanocavity resonance and the second-order IST. The corresponding Rabi splitting at the anti-crossing condition (750 nm wide Au strip) is ~3.8 THz (~128 cm^{-1}), which is approximately 10% of the second-order IST frequency. To the best of our knowledge, this is the first demonstration of strong coupling involving an individual MIR IST between two higher-order subbands in SQW structures. We also fabricated

a set of single nanocavity structures of the same designs on glass substrate and characterized their reflection spectra, which are shown in Figure S2 in the Supporting Information. The resonance positions in the reflection spectra of the single nanocavity structures match those of the nanocavity arrays very well, which suggests that the observed strong coupling between the SQW ISTs and the nanocavity resonance occurs on the single nanocavity level.[35]

Note that for an infinitely deep QW, the single-particle oscillator strength of the IST between the n-th and the m-th subbands is given by $f_{mn} = \frac{64}{\pi^2}\frac{m^2n^2}{(m^2-n^2)^3}$.[23] In this approximation, the second-order IST has a significantly larger oscillator strength than that of the first-order IST, which would facilitate reaching the strong coupling regime. For an actual QW with a finite depth, this analytical result may not be accurate enough, and the oscillator strength difference between the two ISTs in the single-particle picture is usually less significant. However, previous studies have shown that the collective nature of the IST excitations transfers the oscillator strength partially from the first-order IST to the second-order IST, and hence the second-order IST can be significantly stronger than the first-order IST.[40,41]

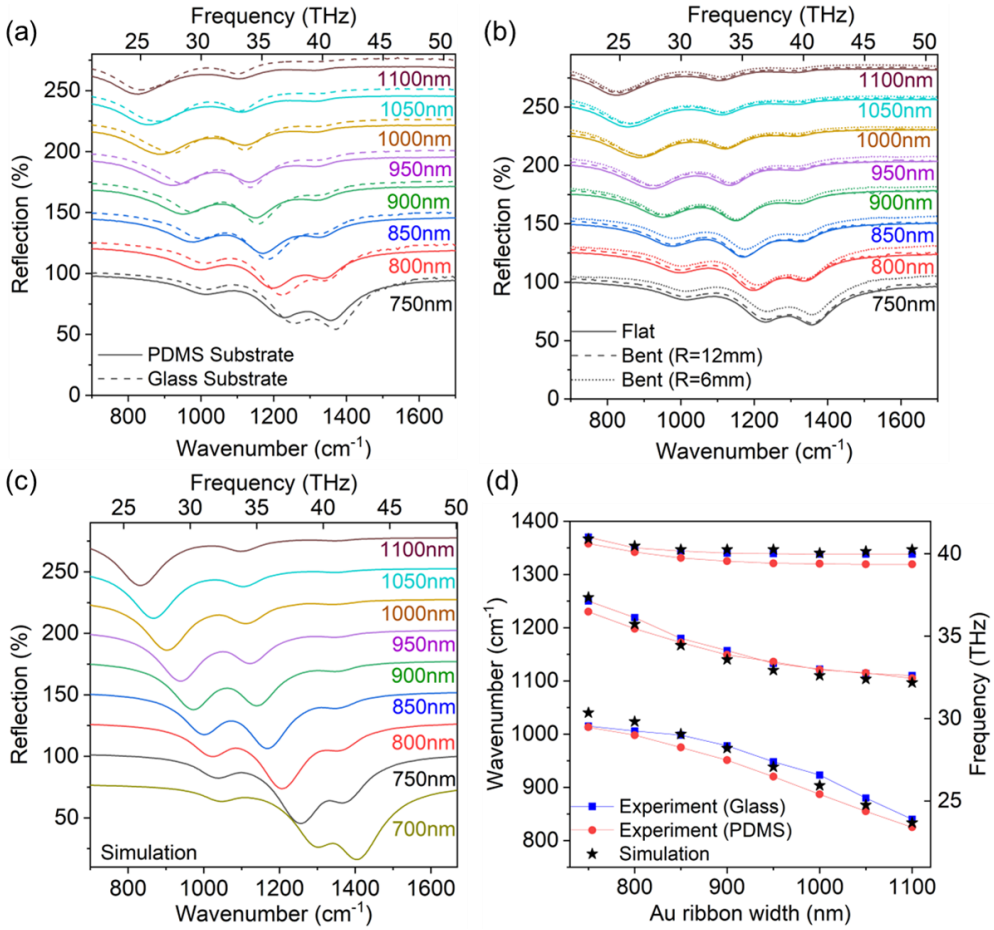

Figure 4 (a) Measured reflection spectra of different patch antenna nanocavity arrays with various Au strip widths on two samples based on the InGaAs SQW: one sample on rigid glass substrate (dashed lines) and another sample on flexible PDMS substrate (solid lines). The array periodicity is twice the Au strip width. The neighboring spectra are offset by 25% along the y-axis. (b) Measured reflection spectra of different patch antenna nanocavity arrays based on the InGaAs SQW on flexible PDMS substrate in three sample configurations: flat, bent with a 12 mm radius, and bent with a 6 mm radius. The neighboring groups of spectra are offset by 25% along the y-axis. Within each group of three spectra (corresponding to the three sample configurations), the spectra are offset by 2% along the y-axis. (c) Simulated reflection spectra of different patch antenna nanocavity arrays with various Au strip widths based on the InGaAs SQW structure. (d) Comparison of the experimentally measured IST polariton frequencies (blue squares and red disks) extracted from (a) with the simulated IST polariton frequencies (black stars) extracted from (c).

The reflection spectra of the sample on PDMS substrate in three different configurations (i.e., flat, bent with 12 mm radius, bent with 6 mm radius) are plotted in Figure 4b. It can be clearly seen that bending of the sample does not alter the reflection spectra significantly. Therefore, our experimental results show that the demonstrated nanocavity structures based on both the GaAs SQW and the InGaAs SQW can be integrated on flexible substrates and withstand significant deformation (bending) without affecting the characteristics of the IST cavity polaritons. Figure 4c shows the simulated reflection spectra of the investigated nanocavity arrays based on the InGaAs SQW, which exhibit good agreement with the experimental spectra. The frequencies of the IST polariton modes were extracted from both the experimental and simulated spectra in Figures 4a-c and plotted in Figure 4d. The typical anti-crossing feature associated with strong light-matter interactions can indeed be observed in the polariton modes originating from both the first-order and second order ISTs. From the values of the Rabi splitting (5.8 THz) and the fitted first-order IST plasma frequency (12.1 THz), the mode overlap factor of the InGaAs SQW f_{SQW} is estimated to be ~23%, which again is in good agreement with the ratio between the SQW thickness (10 nm) and the total thickness of the semiconductor heterostructure inside the nanocavity (43 nm).

In summary, we experimentally demonstrated ultrastrong coupling between the IST in an SQW and the resonant mode of patch antenna nanocavities at room temperature. The Rabi splitting reaches 24% of the IST frequency in a GaAs SQW, which is the largest normalized coupling strength achieved for MIR IST cavity polaritons in an SQW. Furthermore, taking advantage of the small thickness of these SQW structures, we successfully implemented for the first time IST cavity polariton systems on flexible substrates and showed that the characteristics of the IST cavity polaritons can be robust to significant structural deformations. Our work paves the way toward future development of highly flexible SQW-based IST polaritonic devices for a range of applications, including soft and wearable photonics.

ASSOCIATED CONTENT

Supporting Information

The Supporting Information is available free of charge.

MBE growth of SQW samples; sample fabrication; sample characterization; additional simulation results; comparison between this work and previous works; and spectral response of single patch antenna nanocavity.

AUTHOR INFORMATION

Corresponding Author

Peter Qiang Liu – Department of Electrical Engineering, University at Buffalo, The State University of New York, Buffalo, NY 14260, USA; Email: pqliu@buffalo.edu

Authors

Puspita Paul – Department of Electrical Engineering, University at Buffalo, The State University of New York, Buffalo, NY 14260, USA

Sadhvikas J. Addamane – Center for Integrated Nanotechnologies, Sandia National Laboratories, Albuquerque, NM 87123, USA

ACKNOWLEDGEMENT

This work is supported in part by the National Science Foundation (NSF) (Award No. ECCS-1847203). This work was performed, in part, at the Center for Integrated Nanotechnologies, an Office of Science User Facility operated for the U.S. Department of Energy (DOE) Office of Science. Sandia National Laboratories is a multimission laboratory managed and operated by National Technology & Engineering Solutions of Sandia, LLC, a wholly owned subsidiary of Honeywell International, Inc., for the U.S. DOE's National Nuclear Security Administration under contract DE-NA-0003525. The views expressed in the article do not necessarily represent the views of the U.S. DOE or the United States Government.

REFERENCES

[1] E. M. Purcell, Spontaneous emission probabilities at radio frequencies, *Phys. Rev.* **1946**, *69*, 681.

[2] S. Haroche, D. Kleppner, Cavity quantum electrodynamics, *Phys. Today* **1989**, *42*, 24.

[3] H. Walther, B. T. H. Varcoe, B.-G. Englert, T. Becker, Cavity quantum electrodynamics, *Rep. Prog. Phys.* **2006**, *69*, 1325.

[4] J. Mckeever, A. Boca, A. D. Boozer, J. R. Buck, H. J. Kimble, Experimental realization of a one-atom laser in the regime of strong coupling, *Nature* **2003**, *425*, 268.

[5] C. Weisbuch, M. Nishioka, A. Ishikawa, Y. Arakawa, Observation of the coupled exciton-photon mode splitting in a semiconductor quantum microcavity, *Phys. Rev. Lett.* **1992**, *69*, 3314.

[6] H. Deng, G. Weihs, C. Santori, J. Bloch, Y. Yamamoto, Condensation of semiconductor microcavity exciton polaritons, *Science* **2002**, *298*, 199.

[7] K. Hennessy, A. Badolato, M. Winger, D. Gerace, M. Atature, S. Gulde, S. Falt, E. L. Hu, A. Imamoglu, Quantum nature of a strongly coupled single quantum dot–cavity system, *Nature* **2007**, *445*, 896.

[8] D. J. Shelton, I. Brener, J. C. Ginn, M. B. Sinclair, D. W. Peters, K. R. Coffey, G. D. Boreman, Strong coupling between nanoscale metamaterials and phonons, *Nano Lett.* **2011**, *11*, 2104.

[9] I. J. Luxmoore, C. H. Gan, P. Q. Liu, F. Valmorra, P. Li, J. Faist, G. R. Nash, Strong coupling in the far-infrared between graphene plasmons and the surface optical phonons of silicon dioxide, *ACS Photonics* **2014**, *1*, 1151.

[10] J. A. Mason, G. Allen, V. A. Podolskiy, D. Wasserman, Strong coupling of molecular and mid-infrared perfect absorber resonances, *IEEE Photon. Techno. Lett.* **2012**, *24*, 31.

[11] A. D. Dunkelberger, B. T. Spann, K. P. Fears, B. S. Simpkins, J. C. Owrutsky, Modified relaxation dynamics and coherent energy exchange in coupled vibration-cavity polaritons, *Nat. Commun.* **2016**, *7*, 13504.

[12] S. J. Srinivasan, A. J. Hoffman, J. M. Gambetta, A. A. Houck, Tunable coupling in circuit quantum electrodynamics using a superconducting charge qubit with a V-shaped energy level diagram, *Phys. Rev. Lett.* **2011**, *106*, 083601.

[13] A. F. Kockum, A. Miranowicz, S. De Liberato, S. Savasta, F. Nori, Ultrastrong coupling between light and matter, *Nat. Rev. Phys.* **2019**, *1*, 19.

[14] C. Ciuti, G. Bastard, I. Carusotto, Quantum vacuum properties of the intersubband cavity polariton field, *Phys. Rev. B* **2005**, *72*, 115303.

[15] A. A. Anappara, S. De Liberato, A. Tredicucci, C. Ciuti, G. Biasiol, L. Sorba, F. Beltram, Signatures of the ultrastrong light-matter coupling regime, *Phys. Rev. B* **2009**, *79*, 201303.

[16] T. Niemczyk, F. Deppe, H. Huebl, E. P. Menzel, F. Hocke, M. J. Schwarz, J. J. Garcia-Ripoll, D. Zueco, T. Hummer, E. Solano, A. Marx, R. Gross, Circuit quantum electrodynamics in the ultrastrong-coupling regime, *Nat. Phys.* **2010**, *6*, 772.

[17] G. Scalari, C. Maissen, D. Turcinkova, D. Hagenmuller, S. De Liberato, C. Ciuti, C. Reichl, D. Schuh, W. Wegscheider, M. Beck, J. Faist, Ultrastrong coupling of the cyclotron transition of a 2D electron gas to a THz metamaterial, *Science* **2012**, *335*, 1323.

[18] W. Gao, X. Li, M. Bamba, J. Kono, Continuous transition between weak and ultrastrong coupling through exceptional points in carbon nanotube microcavity exciton–polaritons, *Nat. Photonics* **2018**, *12*, 362.

[19] A. Vasanelli, Y. Todorov, C. Sirtori, Ultra-strong light–matter coupling and superradiance using dense electron gases, *C. R. Phys.* **2016**, *17*, 861.

[20] J. Faist, F. Capasso, D. L. Sivco, C. Sirtori, A. L. Hutchinson, A. Y. Cho, Quantum cascade laser, *Science* **1994**, *264*, 553.

[21] P. Q. Liu, A. J. Hoffman, M. D. Escarra, K. J. Franz, J. B. Khurgin, Y. Dikmelik, X. Wang, J.-Y. Fan, C. F. Gmachl, Highly power-efficient quantum cascade lasers, *Nat. Photonics* **2010**, *4*, 95.

[22] K.-K. Choi, B. F. Levine, C. G. Bethea, J. Walker, R. J. Malik, Multiple quantum well 10 μm GaAs/$Al_xGa_{1-x}As$ infrared detector with improved responsivity, *Appl. Phys. Lett.* **1987**, *50*, 1814.

[23] H. Schneider, H. C. Liu, *Quantum Well Infrared Photodetectors: Physics and Applications*, Springer, Berlin, **2007**, 13-77.

[24] L. Sapienza, A. Vasanelli, R. Colombelli, C. Ciuti, Y. Chassagneux, C. Manquest, U. Gennser, C. Sirtori, Electrically injected cavity polaritons, *Phys. Rev. Lett.* **2008**, *100*, 136806.

[25] M. Geiser, G. Scalari, F. Castellano, M. Beck, J. Faist, Room temperature terahertz polariton emitter, *Appl. Phys. Lett.* **2012**, *101*, 141118.

[26] P.-B. Vigneron, S. Pirotta, I. Carusotto, N.-L. Tran, G. Biasiol, J.-M. Manceau, A. Bousseksou, R. Colombelli, Quantum well infrared photo-detectors operating in the strong light-matter coupling regime, *Appl. Phys. Lett.* **2019**, *114*, 131104.

[27] G. Gunter, A. A. Anappara, J. Hees, A. Sell, G. Biasiol, L. Sorba, S. De Liberato, C. Ciuti, A. Tredicucci, A. Leitenstorfer, R. Huber, Sub-cycle switch-on of ultrastrong light–matter interaction, *Nature* **2009**, *458*, 178.

[28] J. Lee, S. Jung, P.-Y. Chen, F. Lu, F. Demmerle, G. Boehm, M.-C. Amann, A. Alù, M. A. Belkin, Ultrafast electrically tunable polaritonic metasurfaces, *Adv. Opt. Mater.* **2014**, *2*, 1057.

[29] D. Dini, R. Köhler, A. Tredicucci, G. Biasiol, L. Sorba, Microcavity polariton splitting of intersubband transitions, *Phys. Rev. Lett.* **2003**, *90*, 116401.

[30] Y. Todorov, A. M. Andrews, R. Colombelli, S. De Liberato, C. Ciuti, P. Klang, G. Strasser, C. Sirtori, Ultrastrong light-matter coupling regime with polariton dots, *Phys. Rev. Lett.* **2010**, *105*, 196402.

[31] P. Jouy, A. Vasanelli, Y. Todorov, A. Delteil, G. Biasiol, L. Sorba, C. Sirtori, Transition from strong to ultrastrong coupling regime in mid-infrared metal-dielectric-metal cavities, *Appl. Phys. Lett.* **2011**, *98*, 231114.

[32] A. Benz, S. Campione, S. Liu, I. Montaño, J. F. Klem, A. Allerman, J. R. Wendt, M. B. Sinclair, F. Capolino, I. Brener, Strong coupling in the sub-wavelength limit using metamaterial nanocavities, *Nat. Commun.* **2013**, *4*, 2882.

[33] R. Sarma, N. Nookala, K. J. Reilly, S. Liu, D. de Ceglia, L. Carletti, M. D. Goldflam, S. Campione, K. Sapkota, H. Green, G. T. Wang, J. Klem, M. B. Sinclair, M. A. Belkin, I. Brener, Strong coupling in all-dielectric intersubband polaritonic metasurfaces, *Nano Lett.* **2021**, *21*, 367.

[34] H. T. Miyazaki, T. Mano, T. Kasaya, H. Osato, K. Watanabe, Y. Sugimoto, T. Kawazu, Y. Arai, A. Shigetou, T. Ochiai, Y. Jimba, H. Miyazaki, Synchronously wired infrared antennas for resonant single-quantum-well photodetection up to room temperature, *Nat. Commun.* **2020**, *11*, 565.

[35] R. Gillibert, M. Malerba, D. Spirito, V. Giliberti, L. Li, A. G. Davies, E. H. Linfield, L. Baldassarre, R. Colombelli, M. Ortolani, Nanospectroscopy of a single patch antenna strongly coupled to a mid-infrared intersubband transition in a quantum well, *Appl. Phys. Lett.* **2020**, *117*, 101104.

[36] A. Delteil, A. Vasanelli, Y. Todorov, C. F. Palma, M. R. St-Jean, G. Beaudoin, I. Sagnes, C. Sirtori, Charge-induced coherence between intersubband plasmons in a quantum structure, *Phys. Rev. Lett.* **2012**, *109*, 246808.

[37] B. Askenazi, A. Vasanelli, A. Delteil, Y. Todorov, L. C. Andreani, G. Beaudoin, I. Sagnes, C. Sirtori, Ultra-strong light–matter coupling for designer Reststrahlen band, *New J. Phys.* **2014**, *16*, 043029.

[38] B. Askenazi, A. Vasanelli, Y. Todorov, E. Saka, J.-J. Greffet, G. Beaudoin, I. Sagnes, C. Sirtori, Midinfrared ultrastrong light–matter coupling for THz thermal emission, *ACS Photonics* **2017**, *4*, 2550.

[39] O. Salihoglu, H. B. Uzlu, O. Yakar, S. Aas, O. Balci, N. Kakenov, S. Balci, S. Olcum, S. Süzer, C. Kocabas, Graphene-based adaptive thermal camouflage, *Nano Lett.* **2018**, *18*, 4541.

[40] R. J. Warburton, C. Gauer, A. Wixforth, J. P. Kotthaus, B. Brar, H. Kroemer, Intersubband resonances in InAs/AlSb quantum wells: selection rules, matrix elements, and the depolarization field, *Phys. Rev. B* **1996**, *53*, 7903.

[41] R. J. Warburton, K. Weilhammer, J. P. Kotthaus, M. Thomas, H. Kroemer, Influence of collective effects on the linewidth of intersubband resonance, *Phys. Rev. Lett.* **1998**, *80*, 2185.

Table of content (TOC) graphic